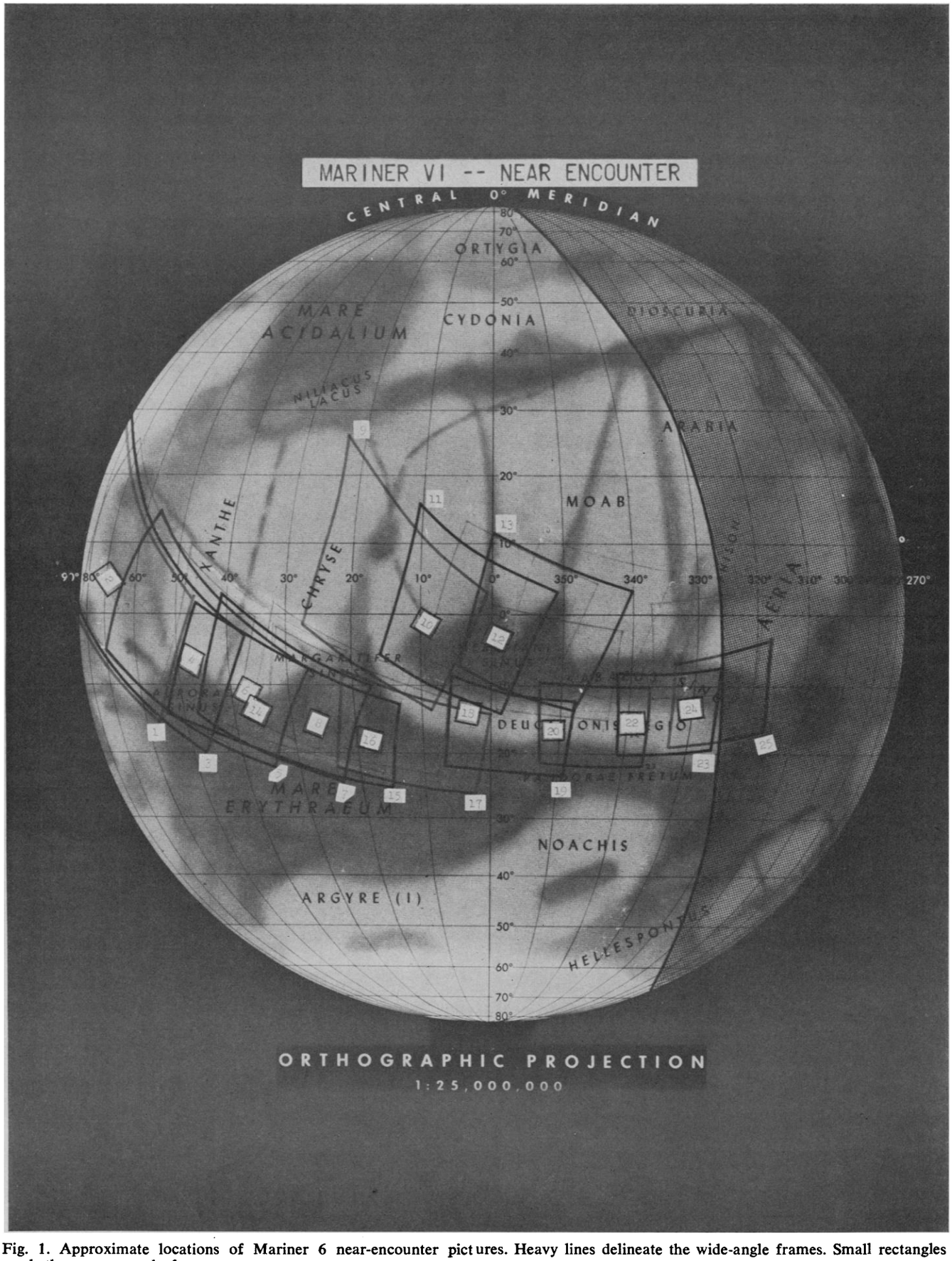

Fig. 1. Approximate locations of Mariner 6 near-encounter pictures. Heavy lines delineate the wide-angle frames. Small rectangles mark the narrow-angle frames.

Reports

Mariner 6 Television Pictures: First Report

In July 1965, Mariner 4 flew past Mars and recorded 20 television pictures of the martian surface; the principal television result of that pioneering flight was the discovery that Mars' surface is heavily cratered and resembles the Moon more than it does the Earth (*1*). On 31 July 1969, the more advanced Mariner 6 spacecraft, carrying two television cameras, passed Mars and recorded 75 pictures. A twin spacecraft, Mariner 7, passed Mars on 5 August 1969. This report summarizes the results of a first, qualitative study of the Mariner 6 television pictures, carried out on the uncalibrated data within a few days after receipt on Earth.

The instrumental characteristics of the Mariners 6 and 7 television camera and data systems are outlined in Table 1; those of Mariner 4 are included for comparison.

In order to maximize the return data within limitation of weight, volume, and especially tape recorder capacity, different kinds of picture data were recorded on two tape recorders. A digital tape recorder was used to store the six least significant bits of an eight-bit (256 level) digitally coded signal from every seventh picture element (pixel) of each picture line, and an analog tape recorder was used to store the analog video signal from each pixel. (The two most significant bits of the eight-bit word were averaged over several lines and were transmitted directly to Earth in real time as a component of the engineering telemetry data stream.) Prior to being recorded, in order to enhance the contrast of small-scale features, the analog signal was automatically controlled to an approximately constant average value and was then passed through a circuit having a cube-law response. Both digital and analog signals were later transmitted to Earth as six-bit digitally encoded signals. The digital data had also been earlier transmitted in real time.

An automatic gain control (AGC) and a contrast pre-emphasis introduce certain characteristic artifacts into the analog data, including severe suppression of spatial frequencies lower than about 10 cycles per TV frame width. These effects will eventually be eliminated, but they are represented within the data presented here.

The planetary encounter period is divided into two parts: a "far-encounter" period beginning 54 hours prior to the time of closest approach (E − 54 hours) and a "near-encounter" period bracketing the time of closest approach. During the period E − 48 hours to E − 28 hours, the narrow-angle camera was used to obtain a series of 33 full-disk analog pictures of Mars, with the AGC inhibited. These pictures were transmitted to Earth from E − 28 hours to E − 25 hours, during the period when the signal could be received at the 210-foot diameter (63 m) antenna of the Goldstone, California station of NASA's deep-space net. A second series of 17 far-encounter pictures was recorded from E−22 hours to E−7 hours. During an 18-minute interval of the near-encounter period, 25 pictures, alternating between cameras A and B, were recorded.

The near-encounter picture fields, superimposed upon a "map" of Mars, are shown in Fig. 1. The particular regions covered by the pictures were chosen to obtain information about the broadest possible range of classical martian features, such as light areas ("deserts"), dark areas ("maria"), seasonally and secularly variable areas, the polar cap, linear markings ("canals"), cloud or frost areas, and circular "deserts."

The data, when completely analyzed, should increase significantly our understanding of the atmosphere and surface of Mars, provide both global and local maps, and, by inference, contribute to a better understanding of the biological status of the planet.

Both cameras operated normally, and the pictures showed no evidence of veiling glare or haze of the kind seen in the Mariner 4 pictures, thus confirming that the optics of the Mariner 4 camera were most likely contaminated with some unknown scattering material. Hence, the previous conclusion that there was a hazy atmosphere extending to altitudes of 150 km was probably unfounded (*2*). The principal results from preliminary study of the Mariner 6 pictures are: the surface of Mars appears similar to that of the Moon, but there are significant differences; some features seen from Earth are characterized; the "blue haze" hypothesis is disproved; and new phenomena associated with the polar cap are discovered.

Even the earliest versions of picture processing permit a preliminary comparison between certain features observed in the Mariner 6 photographs and those which have been recorded by ground-based observations.

In general, we conclude that the appearance of the maria (large, dark areas) more closely resembles that seen in the better telescopic photographs than that in the hand-drawn renditions of most visual observers. With a few notable exceptions, visual observers have tended to represent the maria with sharp angular outlines, while photographs have shown diffuse, somewhat irregular boundaries. As seen in Figs. 2 to 6 the maria indeed show diffuse, irregular edges with a mottled appearance within.

Telescopic photographs, particularly those taken in blue or green light, often show bright areas referred to as "blue" or "white" clouds. It is a characteristic of these features that they exhibit diurnal and perhaps seasonal variations, becoming more enhanced throughout the martian day to a degree that seems to vary from one apparition to the next. Examples include the Tharsis-Candor "W-cloud" and Nix Olympica. Nix Olympica and parts of the "W-cloud" are clearly seen in the Mariner 6 far-encountered sequence. Nix Olympica has been identified in Fig. 2 as a large white-rimmed crater approximately 500 km in diameter with a bright central spot (see arrow). Figure 2 also shows several bright irregular features in Tempe near the evening (right-hand) limb along the edge of the north polar "haze." Telescopic photographs show

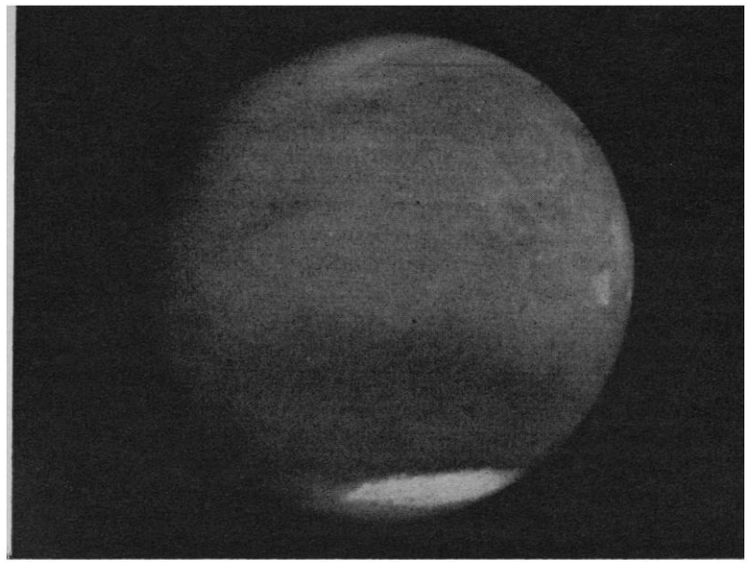

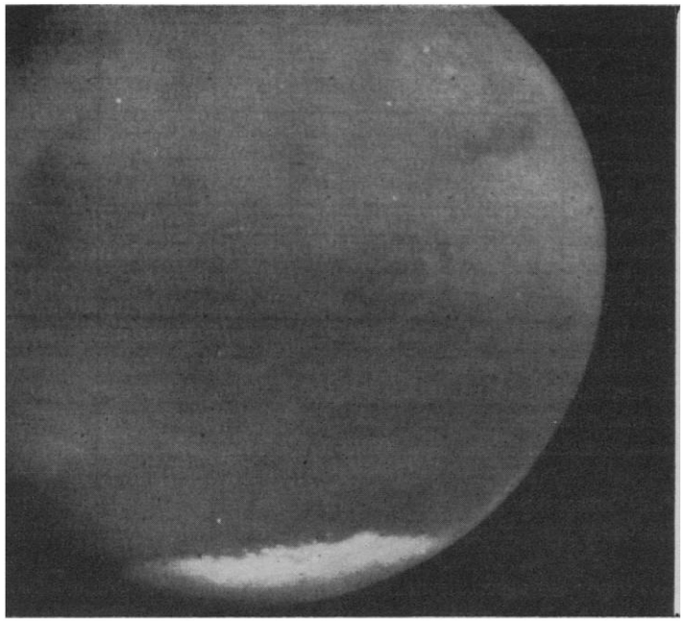

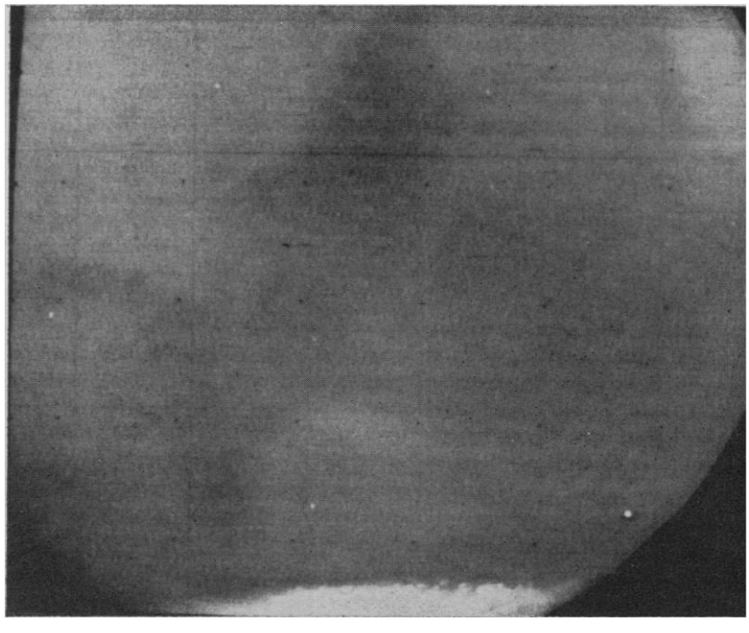

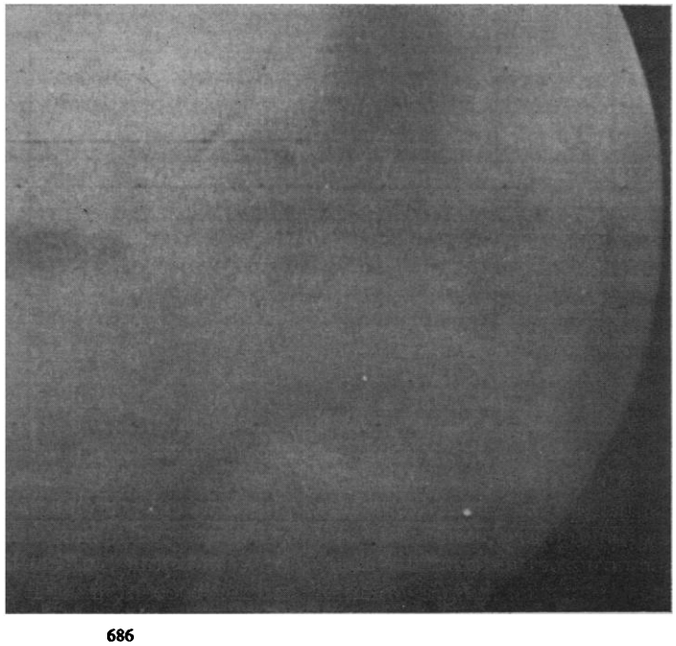

Figs. 2 to 6. The phase angles are 25°. The approximate subspacecraft latitudes are −6°.

Distance to martian surface (km)	Time of picture G.M.T. 7/30/69 (hr : min)	Central meridian east longitude (3)	Typical features
	Fig. 2 (top left); far-encounter frame number, 35		
537,000	08 : 36	224.5°	Mare Sirenum, Tharsis
	Fig. 3 (top right); far-encounter frame number, 35		
453,950	11 : 48	177.8°	Mare Sirenum, Mare Cimmerium, Amazonis
	Fig. 4 (center left); far-encounter frame number, 44		
324,900	16 : 46	105.6°	Syrtis Major, Mare Tyrrhenum, Elysium
	Fig. 5 (center right); far-encounter frame number, 47		
252,150	19 : 34	65.0°	Syrtis Major, Hellas
	Fig. 6 (bottom left); far-encounter frame number, 49		
203,600	21 : 26	38.1°	Syrtis Major, Sabaeus Sinus

that the Tempe "cloud" also exhibits diurnal brightening. Figure 3 shows three end points of the "W" near the afternoon limb. The most westerly of these features is a roughly circular region, some 560 km in diameter. It is observed to brighten steadily as it approaches the limb. Near the center of the disk, this particular spot is as dark as, or slightly darker than, its surroundings. This diurnal behavior might be expected from convective clouds of H_2O, but the region exhibits no cloud-like structure during this brightening. Although the best resolution at which it can be seen is only about 35 km, some individual cloud clusters, waves, or streakiness might be seen in convective clouds at this scale. The structureless uniform brightening—seen on both days of far-encounter—and sharply defined, rather angular edges suggest that it is not caused by atmospheric convection but could be due to the photometric function of this area. However, the brightening of this region at the limb and not at the terminator, as observed in ground-based photographs, means that the function would have to violate the reciprocity principle. Furthermore, ground-based photographs show the region to be brighter in the afternoon than in the morning. A number of bright streaks north and west of the "W" are quite possibly responsible for the general brightening of the Tharsis region as seen in telescopic photographs. Although the streaks bear a certain resemblance to the lunar bright-ray system, their true nature is not known at this time.

It is well known that the dark maria are usually not visible on photographs taken in blue light, although occasionally they are visible with rather low contrast during a "blue clearing." To explain the absence of dark features in blue light, some astronomers have invoked the idea of a "blue haze," a layer of suspended particles that absorbs blue light and hides surface features. Mariner 6 near-encounter photographs taken through a blue filter clearly show craters on the martian surface, thus refuting the existence of such an atmospheric blue haze. Photographs taken at the New Mexico State University Observatory only 2 hours before encounter show that no "blue clearing" was in progress at that time. The mechanism responsible for "blue clearing" is still unknown, but it appears that it must be a surface phenomenon as was originally believed.

Figures 4 and 5 reveal two important new characteristics of the south polar cap region. The north edge of the cap is very sharp, but irregular. Several circular areas, resembling craters, appear along the edge: a particularly prominent one, nearly 130 km in diameter, can be clearly seen near the center of the cap edge in Fig. 5. Close inspection near the afternoon limb (right) reveals craterlike structure within the cap region itself. These features rotate with the planet and exhibit no diurnal variations nor any apparent changes between the first and second days of the far-encounter phase, confirming that at least the periphery of the polar cap is on the surface and not in the atmosphere. The second new feature revealed in the cap region in Figs. 2 and 4 is the marked darkening of the cap area near the south limb. As these frames show, it does not rotate with the planet. One possible interpretation of this feature is that it is a thin, varying atmospheric haze. The Mariner 7 photographic (and other instrumental) program has been revised on the basis of these pictures to provide maximum coverage of the south polar cap.

Table 1. Nominal instrumental characteristics of Mariners 4, 6, and 7 television camera and data systems.

Item	Mariner 4	Mariners 6 and 7	
		Camera A	Camera B
	Optics		
Aperture (mm)	60	10	200
Focal length (mm)	305	52	508
T-number	8	6.5	3.6, 3.84
Type	Simple Cassegrain	Lens	Equal-radii Schmidt Cass.
Shutter	4-Position rotary	4-Position rotary	2-Blade right-left
Exposure (m sec) ("fast"; "slow")	85;200	90;180	6;12
Filters (eff. wavelength, nm)	R 600 G 540	R 573 G 526 B 469	560
	Picture		
Absolute size (mm)	5.5 × 5.5	9.6 × 12.3	9.6 × 12.3
Angular field (deg)	1.1 × 1.1	11 × 14	1.1 × 1.4
Resolution elements ("pixels")	200 × 200	704 × 935	704 × 935
Frame readout time (sec)	24	42.25	42.25
Picture interval (sec)	48	84.5	84.5
Encoding levels $N = 2^n$	$n = 6$	$n = 8$	$n = 8$
	Tape recorders		
		Digital	Analog
Number	1	1	1
Tracks	4	4	4
Tape length (m)	100	110	110
Stored bits (effective)	5×10^6	1.3×10^7	1.2×10^8
Tape speed (cm sec^{-1})			
Record	32.5	30	30
Playback	0.025	4.3	4.3
	Data transmission rates		
(As used) bit sec^{-1}	8 1/3	16.2×10^3	16.2×10^3
(Backup) bit sec^{-1}		270	270

Preliminary study of Mariner 6 near-encounter photographs, like those displayed in Figs. 7 to 10 reinforces the conclusion derived from Mariner 4 that the surface of Mars is more Moon-like than Earth-like. Nonetheless, these Mariner 6 photos also suggest subtle and possibly highly significant differences.

Mars is clearly Moon-like in the abundance, form, arrangement, and sizes of craters. A preliminary count identifies 156 certain craters within the 625,000 km^2 of frame 21 ranging from 3 to 240 km in diameter. The true number is obviously much greater, as narrow-angle frames 20 and 22 covering parts of the same area reveal many more craters down to 300 m in diameter. Various degrees of preservation are seen within this crater population. Preliminary data also suggest a break in the size-distribution curve of craters on at least some parts of Mars which is not recognized in lunar crater populations. These differences would seem to be the result of some weathering and transportational processes that are more effective on Mars than on the Moon.

In detail some martian craters duplicate lunar craters in having slump blocks and terrace as well as radial dry-debris avalanche chutes on steep inner faces. Central peaks, polygonal outlines, blocky ejecta rims, and irregular ejecta sheets are also seen, just as on the Moon. Another Moon-like feature is the irregularly sinuous

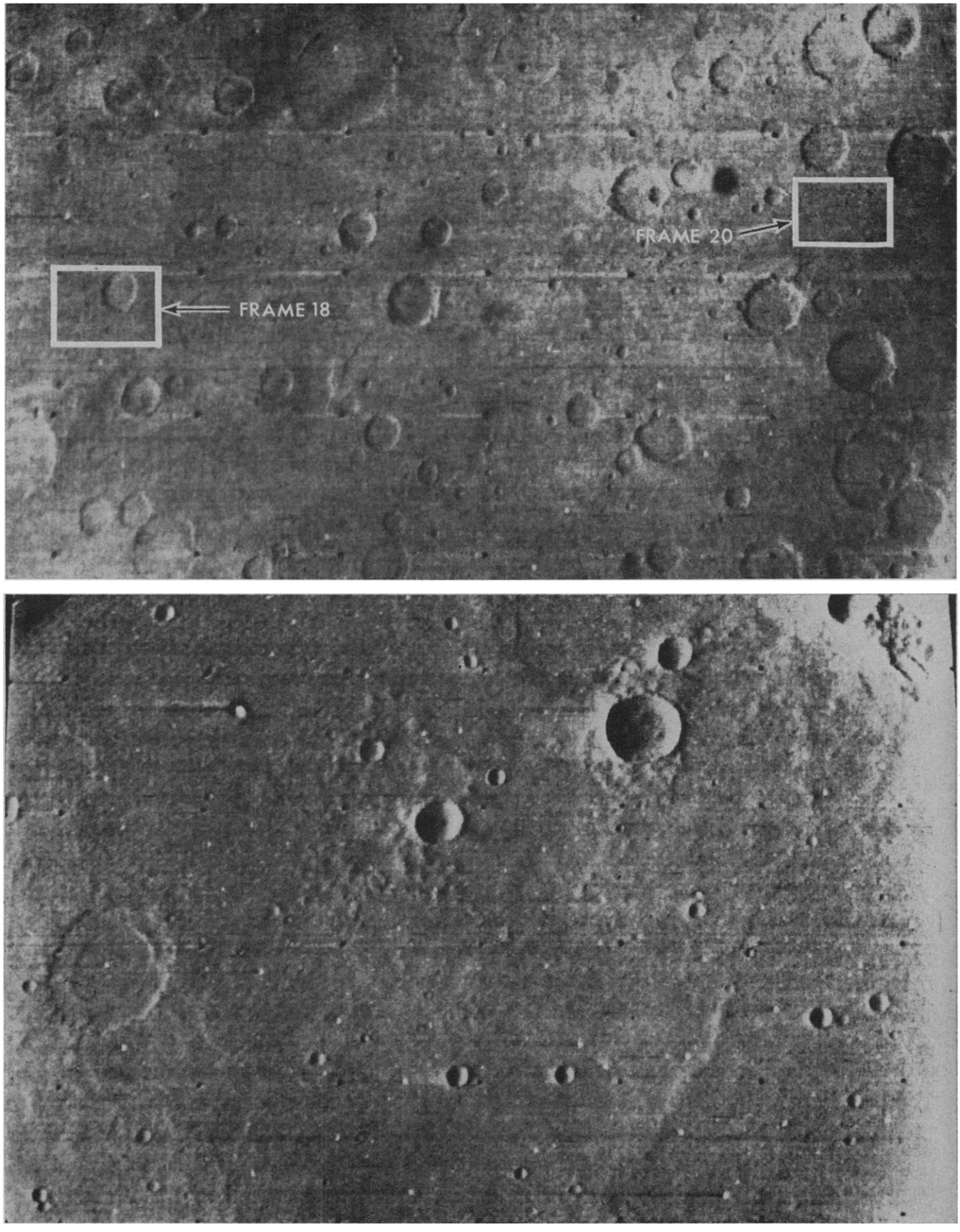

Figs. 7 to 10. Figures 7 and 9 (frames 19 and 21 of the Mariner 6 near-encounter series) are wide-angle photos with overlap on their inner edges and a resolution of about 3 km. Figures 8 and 10 (frames 20 and 22, respectively) cover the small areas shown in Figs. 7 and 9 with a resolution of about 300 m. All photos are within the bright area Deucalionis Regio south of Sabaeus Sinus in the eastern part of the Mariner 6 near-encounter path, approaching the evening terminator. North is at the top.

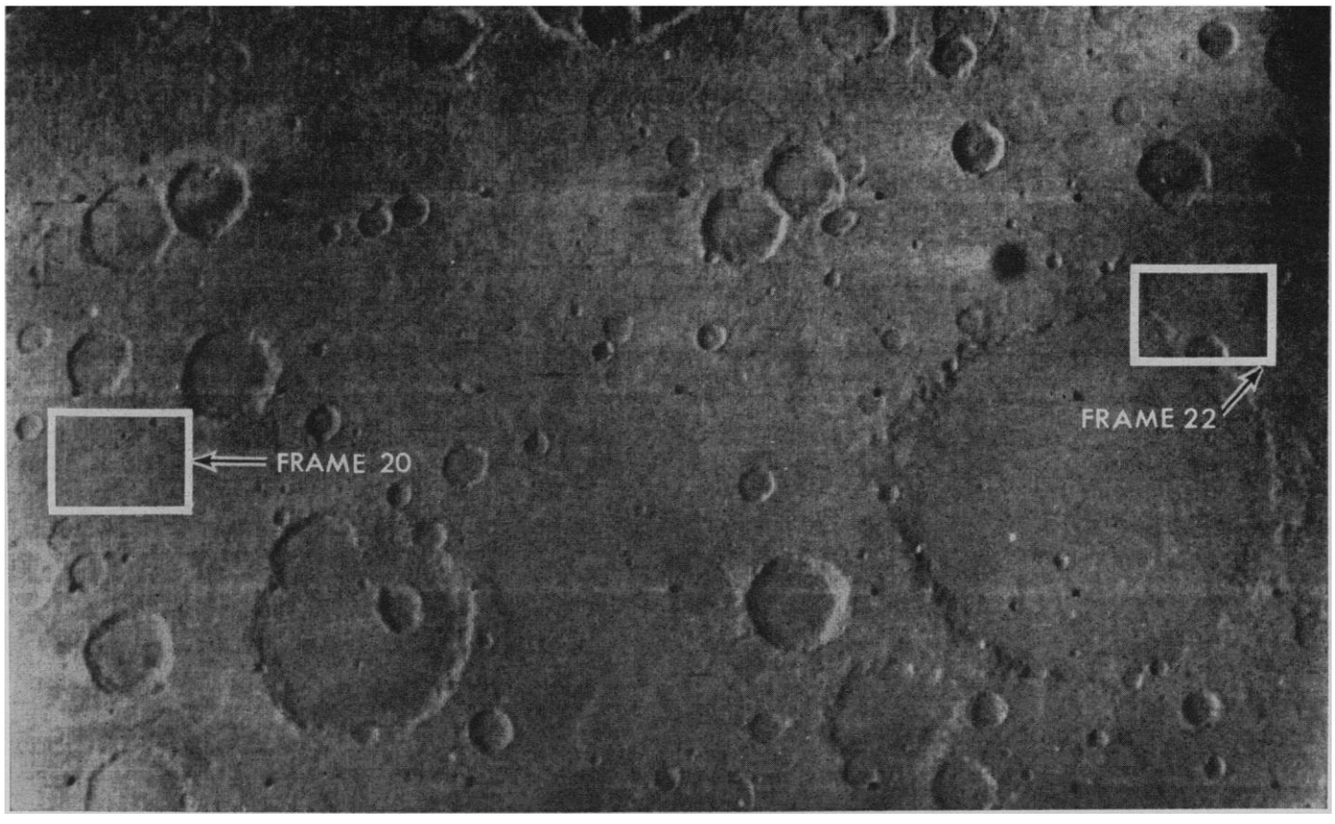

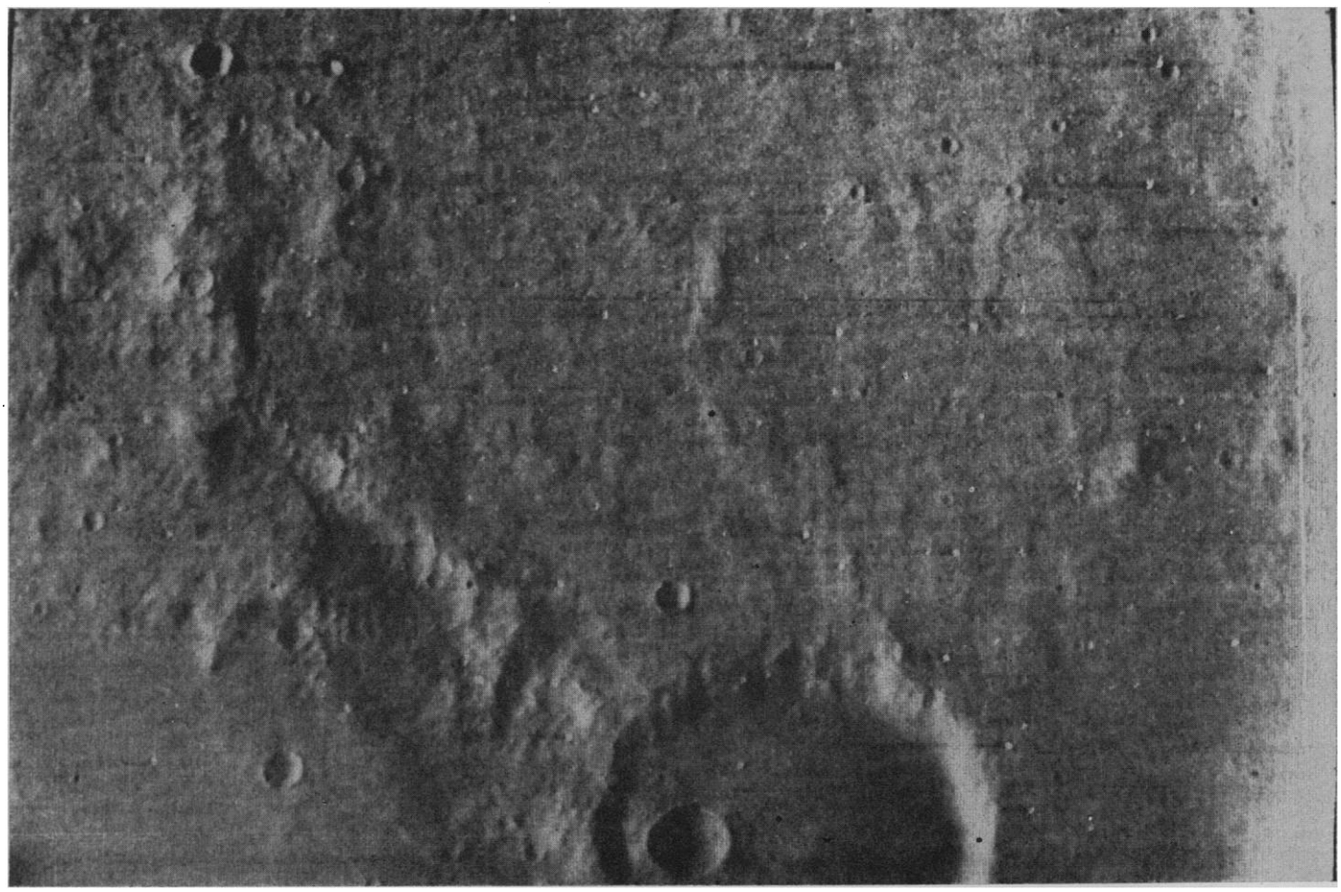

	Near-encounter frame number	Filter	Distance to martian surface (km)	Mars coordinates (*3*)	North-south by east-west dimensions (km)	Viewing angle from vertical	Solar zenith angle (deg)
Fig. 7	19	Green	3613	17°S, 3.2°E	717 × 994	24.4°	58.6°
Fig. 8	20	Minus blue	3544	16.6°S, 9.0°E	73 × 88.5	20.4°	64.3°
Fig. 9	21	Red	3499	16.2°S, 15.1°E	697 × 899	16.4°	70.4°
Fig. 10	22	Minus blue	3497	15.3°S, 20.6°E	72 × 84	15.0°	75.8°

ridges faintly seen extending northward through both Figs. 8 and 9.

Differences between lunar and martian terrains lie in the seemingly more subdued relief of many martian craters, their flatter floors, fewer central peaks, more subdued debris blankets, absence of obvious secondary craters and rays, and possibly greater abundance of "ghost" craters. A striking double concentric "ghost," similar to prominent double concentric craters seen on the back side of the Moon is faintly visible in the western part of Fig. 8. A more facile isostatic adjustment of the martian crust could also be a contributing factor.

No sinuous rilles have yet been identified on the Mariner 6 photos. Furthermore, no distinctive Earth-like phenomena such as mountain ranges, tectonic basins, streamcut topographs, dune fields, playa flats, or other arid-region features have been recognized. On the other hand, a remarkable variety of albedo markings are apparent in the encounter photographs at high solar angle. Such albedo markings, however, are particularly susceptible to spurious effects in the present preliminary form, and their analysis must await reconstruction of the digital and analog data.

ROBERT B. LEIGHTON
NORMAN H. HOROWITZ
BRUCE C. MURRAY, ROBERT P. SHARP
California Institute of Technology, Pasadena 91103

ALAN G. HERRIMAN
ANDREW T. YOUNG
Jet Propulsion Laboratory, Pasadena California 91103

BRADFORD A. SMITH
New Mexico State University, Las Cruces 88001

MERTON E. DAVIES
RAND Corporation, Santa Monica, California 90406

CONWAY B. LEOVY
University of Washington, Seattle 98055

References and Notes

1. R. B. Leighton, B. C. Murray, R. P. Sharp, J. D. Allen, R. K. Sloan, *Science* **149**, 627 (1965).
2. A. T. Young, *Bull. Amer. Astron. Soc.* **1**, 218 (1969).
3. Longitude measured eastward on Mars from the standard ephemeris zero meridian. Ephemeris longitude is measured westward from this meridian.
4. We acknowledge the support and encouragement of the National Aeronautics and Space Administration. We also thank the Mariner Mars '69 project manager, H. M. Schurmeier, and his staff at the Jet Propulsion Laboratory, California Institute of Technology, without whose skill, expert knowledge, and devoted labor Mariner 6 could not have succeeded.

5 August 1969

Methane-Derived Marine Carbonates of Pleistocene Age

Abstract. *In some calcium carbonate–bearing sandstones from the edge of the continental shelf off the northeast United States, the δC^{13} range is from −30 and −60 per mil for both aragonite and high-magnesium calcite. The δC^{13} of coexisting shells of* Modiolus *sp. is normal (+ 1.7 to − 2.7 per mil). The δO^{18} values of around + 3.5 per mil in all samples suggest deposition at temperatures around 0°C. Quaternary methane oxidized either chemically or microbiologically to carbon dioxide is the probable source of carbon in these carbonates.*

Aragonite and high-magnesium calcite in sandstones dredged from five localities on the continental margin off the northeastern United States show stable isotope characteristics that (i) exhibit the largest negative values for δC^{13} yet reported for calcium carbonates; (ii) suggest a possible new mechanism of submarine lithification; (iii) confirm inorganic rather than biogenic precipitation of marine aragonite; (iv) confirm lowered sea temperatures during the last glacial maximum; and (v) exhibit the chemical aggressiveness of dissolved carbonates in corroding silicates and quartz and depositing carbonates in their place.

The aragonite-bearing rocks are slabs having irregular surfaces and numerous cavities lined with layers of clear aragonite in groups of radiating crystals (Fig. 1, top). Slightly agape valves of three specimens of *Modiolus* sp. with periostracum largely intact and a crab shell were enveloped and partially filled with such layers of aragonite.

Aragonite also occurs as masses, spherulites, or cementing matrix and accounts for as much as 50 percent of the total rock. Many feldspar and quartz grains are corroded or replaced by carbonates, and relic outlines of the original grain boundaries can be observed. Figure 1 (bottom) illustrates a common feature in which parts of the original grain persist; the twinning of the feldspar indicates the original continuity of the remnants.

Globorotalia truncatulinoides in sample 2715 (Table 1), the ostracode *Muellerina canadensis* (Brady) in sample 2689, and a C^{14} date of 20,000 years ago for the clear aragonite of sample 2715 indicate a Pleistocene age for these rocks.

The two samples containing high-magnesium calcite (about 14 mole percent $MgCO_3$) are from the northern part of Georges Bank; one, an irregularly shaped carbonate cemented sand, is from an unknown location in the northwest part of the bank; the other (AB4-67-12-174) is from the northeast part of the bank and is one of several flat (about 5 mm thick) concretion-like sandy plates, up to 10 cm in diameter. Neither sample has lined cavities like those of the aragonite-bearing rocks.

Distribution of particle sizes in the residue insoluble in acetic acid of two samples of gray sandy material from sample 2715 showed good sorting around a median size of about 0.35 mm for one sample, and poor sorting around a median size of about 0.2 mm for a sample containing clay. An x-ray analysis of the clay fraction showed dominant chlorite and mica with a trace of montmorillonite. The coarser fractions contained mainly quartz with about 10 percent feldspar.

Isotope data was obtained with a Nier-McKinney type of dual-collecting mass spectrometer (Nuclide Instrument). Carbon isotope data are reported as per mil deviation to the PDB_1—Chicago belemnite standard (*1*, *2*):

$$\delta C^{13} = [(R/R_{ST}) - 1] \times 1000$$

where R represents the ratio of C^{13} to C^{12} in the sample, and R_{ST} the ratio in the standard. Similarly δO^{18} is defined in terms of the ratio of O^{18} to O^{16}.

Our carbonate samples (Table 1) are depleted in C^{13} to about the same extent as certain carbonates associated with sulfur-evaporite domes (*3*) or oxidized hydrocarbons (*4*). Most methanes are more depleted in C^{13} than other natural compounds (*5*), although some methanes that have isotopically equilibrated with CO_2 at elevated temperatures show less depletion in C^{13}; the gases from hot springs in Yellowstone National Park represent such a case ($\delta C^{13} = -8$ to -28) (*1*). Methanes analyzed from marine and brackish deposits near Woods Hole have δC^{13} values between −55 and −60 per mil.

Figure 2 is based on more than 5000 analyses of carbon (*6*). Two characteristics are apparent: (i) carbonates extend over a wide range in δC^{13}; and (ii) the most oxidized carbon, that is, carbonates and the various CO_2 species, are enriched in C^{13} by comparison with reduced carbon, that